THE JOURNAL OF PHYSICAL CHEMISTRY Letters

Letter

pubs.acs.org/JPCL

Rotational Doppler Effect: A Probe for Molecular Orbitals Anisotropy

Quan Miao,[†,‡,§] Oksana Travnikova,[‡,⊗] Faris Gel'mukhanov,[†,‡] Victor Kimberg,[†,‡] Yu-Ping Sun,[†,∥] T. Darrah Thomas,[⊥] Christophe Nicolas,[‡] Minna Patanen,[‡] and Catalin Miron*[,‡,#]

[†]Theoretical Chemistry and Biology, School of Biotechnology, Royal Institute of Technology, Roslagstullsbacken 15, S-10691 Stockholm, Sweden

[‡]Synchrotron SOLEIL, l'Orme des Merisiers, Saint-Aubin, BP 48, 91192 Gif-sur-Yvette Cedex, France

[§]College of Electronics, Communication and Physics, Shandong University of Science and Technology, Qianwangang Road 579, Qingdao 266590 Shandong, People's Republic of China

[∥]School of Science, Shandong University of Technology, Xincunxi Road 266, ZiBo, 255049 Shandong, China

[⊥]Department of Chemistry, Oregon State University, 153A Gilbert Hall, 2100 SW Campus Way, Corvallis, Oregon 97331, United States

[#]Extreme Light Infrastructure - Nuclear Physics (ELI-NP), "Horia Hulubei" National Institute for Physics and Nuclear Engineering, 30 Reactorului Street, RO-077125 Măgurele, Jud. Ilfov, Romania

ABSTRACT: The vibrationally resolved X-ray photoelectron spectra of $X^2\Sigma_g^+(3\sigma_g^{-1})$ and $B^2\Sigma_u^+(2\sigma_u^{-1})$ states of N_2^+ were recorded for different photon energies and orientations of the polarization vector. Clear dependencies of the spectral line widths on the X-ray polarization as well as on the symmetry of the final electronic states are observed. Contrary to the translational Doppler, the rotational Doppler broadening is sensitive to the photoelectron emission anisotropy. On the basis of theoretical modeling, we suggest that the different rotational Doppler broadenings observed for gerade and ungerade final states result from a Young's double-slit interference phenomenon.

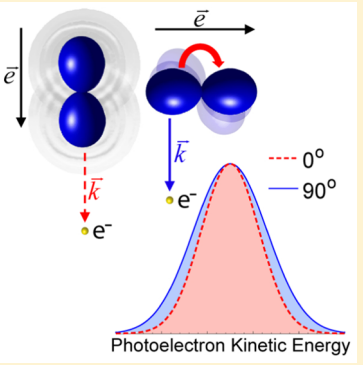

The Doppler effect,[1,2] a shift in frequency of the emitted waves by a moving source, is a phenomenon with numerous applications in science and technology. The well-known motion-related broadening of the lines in electron spectroscopy is attributed to the fundamental physical phenomenon of electronic translational Doppler effect.[3−14] It can be easily understood from the direct analogy to the conventional, acoustical, or electromagnetic Doppler effect. The translational Doppler broadening, resulting from the velocity distribution of the outgoing electron relative to the drift velocity of the emitting atom/molecule, depends ultimately only on the mass of the emitting atoms and molecules, on their temperature, and on the momentum of the photoelectron, **k**, and therefore is almost the same for all valence photoemission lines in the X-ray region; however, Sun et al. predicted[15] that due to the recoil angular momentum **j** the X-ray photoemission lines are strongly affected by a rotational Doppler broadening (RDB), which is of the same order of magnitude as its translational counterpart. The effect was experimentally confirmed in molecular nitrogen[16] and was further explored in hydrogen chloride.[17] Rotational Doppler effects associated with the orbital angular momentum of the light beam[18] and spin of the photon[19] were also observed in optical spectroscopy. We address a new and unexplored facet of the rotational Doppler effect: its angular and state dependence.

Despite the similarity between the translational and rotational Doppler effects, there is a fundamental, qualitative difference between them. Contrary to the translational Doppler shift, the rotational Doppler shift is proportional to the recoil angular momentum, which depends on the angle $\theta = \angle(\mathbf{R},\mathbf{k})$ between the internuclear radius vector, **R**, and **k**. The photoionization cross section depends on the mutual orientation of the vectors **R**, **k**, and **e** (the polarization vector of the X-rays), and this dependence is different for different final states. As a consequence, the RDB is different for different final cationic states, and the associated spectral line widths vary with the polarization of the exciting X-rays. Our present photoelectron spectroscopy measurements for the nitrogen molecule (Figure 1) directly probe the molecular orbitals' anisotropy, providing the very first evidence of the strong dependence of the RDB on both the final electronic state and on the angle $\chi = \angle(\mathbf{e},\mathbf{k})$ between the polarization vectors **e** and **k**. Here we focus on the state-specific polarization dependence

Received: February 12, 2015
Accepted: April 9, 2015
Published: April 9, 2015

DOI: 10.1021/acs.jpclett.5b00325
J. Phys. Chem. Lett. 2015, 6, 1568−1572

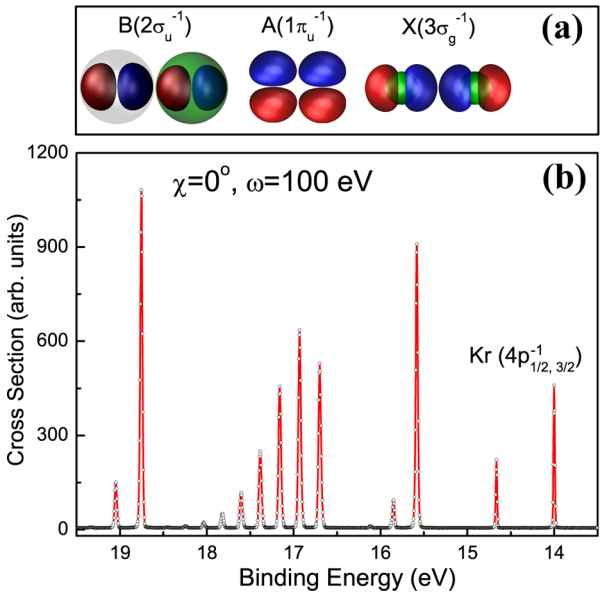

Figure 1. (a) Isosurfaces of the atomic orbitals (AOs) contributing to the studied molecular orbitals (red and blue: 2p AOs, white and green: 2 s AOs). (b) Experimental X-ray photoelectron spectrum of N_2 plotted against binding energy, $\omega - E_{el}$. The vibrational progressions of the $X^2\Sigma_g^+(3\sigma_g^{-1})$, $A^2\Pi_u(1\pi_u^{-1})$, and $B^2\Sigma_u^+(2\sigma_u^{-1})$ final states are observed.

of the Doppler broadening of the $X^2\Sigma_g^+(3\sigma_g^{-1})$ and $B^2\Sigma_u^+(2\sigma_u^{-1})$ cationic states of N_2, whose ionization potentials are $I_i \approx 15.5$ and 18.6 eV ($i = \sigma_g,\sigma_u$), respectively. We will not analyze the rotational broadening of the $A^2\Pi_u(1\pi_u^{-1})$ photoemission lines because they are "contaminated" by a large spin−orbit splitting $\Delta_{SO} = 9.25$ meV.[20,21]

The RDB is found by subtracting the instrumental and translational Doppler broadenings from the experimental line widths. The obtained data show the dependence of the RDB on the X-ray polarization and on the final state. To determine the instrumental broadening at the different X-ray energies used, we simultaneously recorded Kr valence photoemission. (See Figure 1.) No RDB is present for atomic lines, and the well-known translational Doppler broadening (12.6 and 18.6 meV at 100 and 200 eV, respectively) has been subtracted from the total spectral line width of the Kr 4p valence photoemission data, revealing instrumental broadenings of about 13 and 17 meV for the photon energies $\omega = 100$ and 200 eV, respectively. Despite a rather small variation of the RDB, the normalized spectral line profiles for the lowest vibrational substates of the two electronic states allow one to explicitly visualize the differences in the RDB for different final states and polarizations. (See Figure 2.)

The X-ray photoionization leads to the ejection of a photoelectron of momentum $\mathbf{k}$, which is transferred to the N_2 molecule of mass M, moving with the velocity $\mathbf{v}$. The X-ray photoemission line is shifted due to the translational Doppler $\mathbf{k}\cdot\mathbf{v}$ and recoil effects $\Delta_{tr} = k^2/2M$.[22−25] At the same time, the ejected electron also transfers to the molecule, rotating with the angular velocity $\mathbf{w}$, an angular momentum $\mathbf{j} = [\mathbf{R}\times\mathbf{k}]/2$, where $\mathbf{R}/2$ is the radius vector of atom with respect to the center of gravity. The recoil angular momentum $j(\theta) = (kR/2)\sin\theta$ with $\theta = \angle(\mathbf{k},\mathbf{R})$ changes the initial angular momentum $\mathbf{J}_0 = \mathbf{w}I \rightarrow \mathbf{J} = \mathbf{J}_0 + \mathbf{j}$, where $I = MR^2/4$ is the moment of inertia. This shifts the photoelectron line, $E_J - E_{J0} = (\mathbf{J}_0 + \mathbf{j})^2/2I - \mathbf{J}_0^2/2I = \mathbf{j}\cdot\mathbf{w} +$

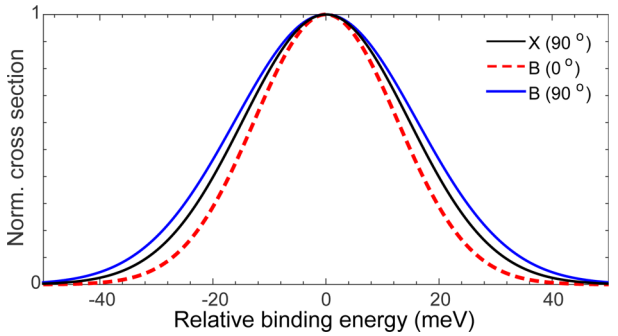

Figure 2. Visualization of the differences in RDB for different electronic states and polarizations. Gaussian fits of the experimental profiles (including all broadenings) are shown normalized to unity at the maximum for the $v = 0$ vibrational substate of the $\sigma_{3\sigma_g}$ (X state) at $\chi = \angle(\mathbf{e},\mathbf{k}) = 90°$ and $\sigma_{2\sigma_u}$ (B state) at $\chi = 0°$, 90°. $\omega = 100$ eV. The profiles are plotted as a function of the relative binding energy with respect to the peak position.

Δ_{rot}, where $\mathbf{j}\cdot\mathbf{w}$ is the rotational Doppler shift[15] (see Figure 3a) while $\Delta_{rot}(\theta) = j^2(\theta)/2I = \Delta_{tr}\sin^2\theta$ is the rotational recoil

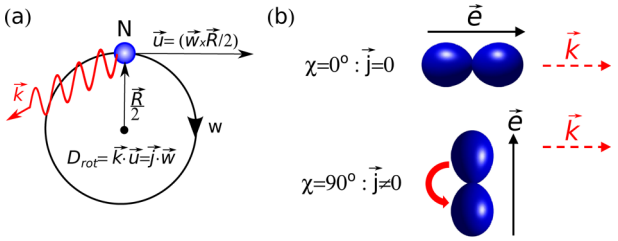

Figure 3. Physical picture of the rotational Doppler broadening. (a) The electron energy is Doppler shifted by $\mathbf{k}\cdot\mathbf{u} = \mathbf{j}\cdot\mathbf{w}$, where $\mathbf{u} = \mathbf{w}\times\mathbf{R}/2$ is the linear velocity of the atom rotating with the angular velocity $\mathbf{w}$ around the molecular center of mass. (b) RDB's dependence on the ejection angle of the photoelectron relative to the polarization vector, $\chi = \angle(\mathbf{k},\mathbf{e})$. The photoionization probability is maximum when the molecule is oriented along the polarization vector. (See the text.) The recoil angular momentum $j(\theta) = (kR/2)\sin\theta \approx (kR/2)\sin\chi$ is suppressed when $\mathbf{k}\|\mathbf{e}$, and it is maximum for the orthogonal geometry $\mathbf{k}\perp\mathbf{e}$. Hence, the RDB is maximum when $\chi = 90°$.

shift.[26−28] An analysis of the angular dependence of $j(\theta)$ and $\sigma_i(\chi,\theta)$ reveals a rather unexpected result: the RDB is different for different final states $|\psi_i^{-1}\rangle$, and it depends on the electron emission angle χ.

To interpret the observed phenomenon, we generalize the photoionization cross section[15] of the molecular orbital (MO) ψ_i by taking into account the θ and χ dependence of $\sigma_i(\chi,\theta) = |\mathbf{e}\cdot\mathbf{d}_i|^2$

$$\sigma_i(\chi, E) = \int_0^\pi d\theta \sin\theta \frac{\sigma_i(\chi,\theta)}{D(\theta)} e^{-\left(\frac{E+\Delta(\theta)}{D(\theta)}\right)^2 4\ln 2} \quad (1)$$

where we use atomic units, $E = E_{el} - (\omega - I_i)$ is the relative kinetic energy, $\mathbf{d}_i$ is the dipole moment of photoionization, $E_{el} = k^2/2$, and $\Delta(\theta) = \Delta_{tr} + \Delta_{rot}(\theta) = \Delta_{tr}(1 + \sin^2\theta)$. The total (rotational and translational) Doppler broadening for randomly oriented molecules $D_i(\chi)$ is the full width at half-maximum (fwhm) of the profile 1. In the molecular frame, the RDB[15] $D_{rot}(\theta) = j(\theta)\bar{w}2(\ln 2)^{1/2} = D_{tr}\sin\theta$, together with the translational Doppler broadening, $D_{tr} = k\bar{v}2(\ln 2)^{1/2} \approx D_{rot} \approx$ 20−30 meV, leads to the total Doppler broadening in the

DOI: 10.1021/acs.jpclett.5b00325
J. Phys. Chem. Lett. 2015, 6, 1568−1572

Table 1. RDB (fwhm) $D^i_{rot}(\chi)$ (in meV) (Experiment/Theory (eq 1)) for the Lowest Vibrational Substates of the X($3\sigma_g^{-1}$) and B($2\sigma_u^{-1}$) Electronic States of N_2^+[a]

ω	width	90°	0°	ΔD^i_{rot}
100	$3\sigma_g^{-1}$: $D^{\sigma_g}_{rot}$	23.9 ± 0.2/22.8	14.4 ± 0.3/14.2	9.5 ± 0.3/8.6
	$2\sigma_u^{-1}$: $D^{\sigma_u}_{rot}$	28.7 ± 0.7/28.6	16.6 ± 0.2/17.4	12.1 ± 0.7/11.2
	ΔD^{ug}_{rot}	4.8 ± 0.7/5.8	2.2 ± 0.3/3.2	
200	$3\sigma_g^{-1}$: $D^{\sigma_g}_{rot}$	33.1 ± 0.3/30.7	21.7 ± 0.3/21.4	11.4 ± 0.4/9.3
	$2\sigma_u^{-1}$: $D^{\sigma_u}_{rot}$	39.0 ± 1.8/34.6	26.6 ± 0.1/25.9	12.4 ± 1.8/8.7
	ΔD^{ug}_{rot}	5.8 ± 1.8/3.9	4.9 ± 0.3/4.5	

[a]In the present case, experimental and theoretical (reaction 1) profiles have, with a good accuracy, a Gaussian shape. Therefore we found the RDB $D^i_{rot}(\chi)$ using equation $D^i_{rot}(\chi) = (D^2{}_i(\chi) - D^2_{tr})^{1/2}$. The translational Doppler broadening for the X state is 21.5/31.7 meV, and for the B state it is 21.1/31.5 meV for ω = 100/200 eV, respectively. In the experiment, the photoelectrons were collected in a cone with the finite acceptance angle $\Delta\chi$ < 38°, while theoretical calculations were performed for the ideal conditions ($\Delta\chi$ = 0°). It can be shown that the deviation related to this approximation cannot exceed 2 $\sin^2(\Delta\chi/4)$< 5%. $\Delta D^{ug}_{rot}(\chi) = D^{\sigma_u}_{rot}(\chi) - D^{\sigma_g}_{rot}(\chi)$, $\Delta D^i_{rot} = D^i_{rot}(90°) - D^i_{rot}(0°)$. The experimental error is given as standard deviation. Preliminary results of our measurements for the X state for χ = 0°, 90° were introduced in the review.[29] The RDB shows a monotonic behavior with the increase im photon energy as a function of the excitation energy.[16]

molecular frame, $D(\theta) = (D^2_{tr} + D^2_{rot}(\theta))^{1/2} = D_{tr}(1 + \sin^2\theta)^{1/2}$. Here $\bar{v} = (2k_BT/M)^{1/2}$ and $\bar{w} = (2k_BT/I)^{1/2}$ are the thermal and angular velocities, respectively, and $\bar{J} = I\bar{w} \approx 10$ is the characteristic rotational level populated in the ground state. The index i was deliberately dropped from $k = (2(\omega - I_i))^{1/2}$ because the related electronic state dependence does not exceed 2% in our case; however, it has been accounted for in the simulations. Contrary to D_{tr}, the RDB $D_{rot}(\theta)$ depends on θ. This θ dependence gives a hint why the RDB for randomly oriented molecules, $D^i_{rot}(\chi)$ (see Table 1), depends on both χ and ψ_i.

The main reason for this dependence is the anisotropy of the $2p_z$ atomic orbital, which contributes differently in different MOs (see also Figure 1a)

$$\psi_i = a_i(2s^{(1)} \pm 2s^{(2)}) + b_i(2p_z^{(1)} \mp 2p_z^{(2)}) \quad (2)$$

where $i = 3\sigma_g, 2\sigma_u$. Contrary to the ionization of the 2s electron with the amplitude $(\mathbf{e}\cdot\mathbf{d}_{2s})$, the ionization of the $2p_z$ electron depends on the orientation of the molecular axis ($\mathbf{R}\|z$) relative to $\mathbf{e}$ and $\mathbf{k}$

$$(\mathbf{e}\cdot\mathbf{d}_{2s}) \propto (\mathbf{e}\cdot\mathbf{k})$$
$$(\mathbf{e}\cdot\mathbf{d}_{2p_z}) \propto (\hat{\mathbf{R}}\cdot\hat{\mathbf{k}})(\mathbf{e}\cdot\hat{\mathbf{k}}) - (\mathbf{e}\cdot\hat{\mathbf{R}})/3 \quad (3)$$

where $\mathbf{d}_{2s}$ and $\mathbf{d}_{2p_z}$ are the photoionization dipole moments of the 2s and $2p_z$ electrons, respectively.

To gain further insight into the physical picture, one should notice that for χ = 0°, 90° the $2p_z$ ionization occurs when the molecular axis is oriented preferentially along $\mathbf{e}$ because in both cases $\sigma_i(\chi,\theta) \propto (\mathbf{e}\cdot\hat{\mathbf{R}})^2$. This means that $j(\theta)$, and hence the RDB, takes maximum and minimum values when $\mathbf{k}\perp\mathbf{e}$ and $\mathbf{k}\|\mathbf{e}$, respectively (Figure 3). Both experiment and theory (Table 1) confirm this qualitative picture: $D^i_{rot}(90°) > D^i_{rot}(0°)$.

The total photoionization amplitude is the coherent sum of the ionization amplitudes for the two equivalent nitrogen atoms,[30] playing the role of the two slits in the Young's double-slit experiment (YDSE)[24,25,31−36]

$$(\mathbf{e}\cdot\mathbf{d}_i) = (\mathbf{e}\cdot\mathbf{d}_i^+)e^{i\mathbf{k}\cdot\mathbf{R}/2} \pm (\mathbf{e}\cdot\mathbf{d}_i^-)e^{-i\mathbf{k}\cdot\mathbf{R}/2} \quad (4)$$

where $\mathbf{d}_i^{\pm} = a_i\mathbf{d}_{2s} \pm b_i\mathbf{d}_{2p_z}$. The major difference between these channels resides in the phase factors $e^{i\mathbf{k}\cdot\mathbf{R}/2}$ and $\pm e^{-i\mathbf{k}\cdot\mathbf{R}/2}$. The related, YDSE or Cohen−Fano (CF), interference term[24,25,31−35] $\sigma^{int}{}_i(\theta,\chi) = 2\mathrm{Re}[(\mathbf{e}\cdot\mathbf{d}_i^+)(\mathbf{e}\cdot\mathbf{d}_i^-)^* e^{i\mathbf{k}\cdot\mathbf{R}}]$ in the cross section $\sigma_i(\theta,\chi) = |\mathbf{e}\cdot\mathbf{d}_i|^2 = \sigma^{dir}{}_i(\chi,\theta) \pm \sigma^{int}{}_i(\chi,\theta)$ (eq 4) has opposite signs for the gerade and the ungerade cationic states. Here $\sigma^{dir}{}_i(\theta,\chi) = |\mathbf{e}\cdot\mathbf{d}_i^+|^2 + |\mathbf{e}\cdot\mathbf{d}_i^-|^2$.

Thus, when $\chi \neq 90°$, the RDB depends on the molecular orbital ψ_i through the mixing coefficients a_i and b_i as well as via the YDSE interference. The calculations for χ = 0°, in agreement with the measurements, clearly show the sensitivity of the RDB to the final state (Table 1). The χ = 90° geometry, where the 2s ionization channel is completely quenched (see eq 3) and the different RDBs observed for the gerade and the ungerade final states (Table 1) are solely caused by the YDSE interference, deserves a special comment. Let us simply estimate $D^{\sigma_{g,u}}_{rot} = (\langle D^2_{rot}(\theta)\sigma_{g,u}\rangle/\langle\sigma_{g,u}\rangle)^{1/2}$, taking into account that $kR \gg 1$ and that the only difference between g- and u-ionization channels $\sigma_{g,u} \propto 1 \mp \cos(\mathbf{k}\cdot\mathbf{R})$ is the interference term.[24,25,31] By neglecting $\langle D^2_{rot}(\theta)\cos(kR\cos\theta)\rangle \approx 1/(kR)^4 \ll 1$ we get $D^{\sigma_{g,u}}_{rot} \approx (\langle D^2_{rot}(\theta)\rangle/\langle 1 \mp \cos(\mathbf{k}\cdot\mathbf{R})\rangle)^{1/2}$. Thus, the difference of RDBs for ungerade and gerade states reads

$$\Delta D^{ug}_{rot} = D^{\sigma_u}_{rot} - D^{\sigma_g}_{rot} \approx -\bar{D}_{rot}\frac{\sin(kR + 2\delta)}{kR} \quad (5)$$

where $\bar{D}_{rot} = \langle D^2_{rot}(\theta)\rangle^{1/2}$ and δ is the scattering phase of photoelectron by the adjacent nitrogen atom.[25] Equation 5 results in $\Delta D^{ug}_{rot} \approx 4.6$ and 4.1 meV for E = 100 and 200 eV, respectively, using $\delta \approx 0.7 - k$. The simple estimate (eq 5), being in a reasonable agreement with the accurate calculations given in Table 1 for two energy values, shows a non-monotonous, oscillatory dependence of ΔD^{ug}_{rot} on energy.

In summary, in this work, we report the experimental observation and the theoretical modeling of the consequences of two physical phenomena: (i) the rotational counterpart of the translational Doppler effect−the rotational Doppler effect and (ii) the quantum indistinguishability of the two atoms in the inversion symmetric nitrogen molecule. We demonstrated for the first time that contrary to the translational Doppler broadening, the RDB depends on the final electronic state. Moreover, we also showed that the former is sensitive to the polarization of the X-rays and to the YDSE interference, which is different for the gerade and the ungerade final states reached by photoionization. The rich physics discussed here for a textbook case, the nitrogen molecule, opens the way to a novel family of studies of the photoionization anisotropy and of the YDSE interferences for a variety of species based on the fascinating properties of the rotational Doppler effect.

DOI: 10.1021/acs.jpclett.5b00325
J. Phys. Chem. Lett. 2015, 6, 1568−1572

METHODS

The experiment was performed at the PLEIADES beamline[37] at SOLEIL, which already allowed us to study the spectral line shapes in photoemission spectra with unprecedented accuracy.[38] The measurements were performed using a VG-Scienta R4000 electron spectrometer mounted with the electron detection axis vertical. X-ray polarization was set at 0 and 90° with respect to this axis. Under the most favorable conditions, with linear vertical polarization (0°) and 100 eV photon energy, the count rate was on the order of 24 kHz at the maximum of X state, and the acquisition time for spectrum shown in Figure 1 was ∼90 min. Pure nitrogen (99.998%) and atomic Kr (99.99%) from Air Liquide were premixed and introduced into the gas cell (VG-Scienta) of the electron energy analyzer. The sample gas pressure in the differentially pumped gas cell was estimated to be on the order of 10^{-3} mbar (molecular density 2.4×10^{13} cm^{-3}), estimated from the measured pressure in the spectrometer vacuum chamber, outside the gas cell of 1×10^{-5} mbar. The gas cell is equipped with a series of electrodes to minimize the effect of plasma potentials. The temperature of the gas was $T = 294 \pm 1$ K. Lifetime broadening of the considered final cationic states is much smaller ($<10^{-8}$ eV[39]) than the Doppler broadening and does not affect our analysis.

Our calculations of the Doppler broadening $D_i(\chi)$ were performed using eqs 1 and 4 according to the method outlined in refs 24 and 25. The atomic ionization cross sections σ_{2s} and σ_{2p} were computed using the data from ref 40. The coefficients in ψ_i (eq 2) ($a_{3\sigma_g} = 0.4$, $b_{3\sigma_g} = 0.6$; $a_{2\sigma_u} = 0.7$, $b_{2\sigma_u} = 0.3$) were calculated with the help of Gaussian 09 package[41] at the DFT level using the B3LYP functional and the 3-21 g basis set.

AUTHOR INFORMATION

Corresponding Author

*E-mail: Catalin.Miron@synchrotron-soleil.fr.

Present Address

⊗(O.T.) CNRS, Laboratoire de Chimie Physique-Matière et Rayonnement, UMR 7614, F-75005 Paris, France; and UPMC Univ Paris 06, UMR 7614, LCPMR, F-75005 Paris, France.

Notes

The authors declare no competing financial interest.

ACKNOWLEDGMENTS

The experiments were performed at the PLEIADES beamline at the SOLEIL Synchrotron radiation laboratory in France (proposal number 99090106). We are grateful to the SOLEIL staff for the smooth running of the facility. O.T. acknowledges the EU 7th Framework Programme (FP7/2007-2013) grant no. 252781, Q.M. acknowledges the National Natural Science Foundation of China (grant no. 11447148) and Shandong Provincial Natural Science Foundation, China (grant no. ZR2014AP001), and Y.-P.S. acknowledges the National Natural Science Foundation of China (grant no. 11204163) and Doctoral Foundation of Shandong Province (BS2013SF018). We also acknowledge support from the European COST action CM1204 - XUV/X-ray light and fast ions for ultrafast chemistry (XLIC) and from the Swedish Research Council (VR). F.G. and C.M. acknowledge funding by a public grant from the Laboratoire d'Excellence Physics Atoms Light Matter (LabEx PALM) overseen by the French National Research Agency (ANR) as part of the Investissements d'Avenir program (ANR-10-LABX-0039).

REFERENCES

(1) Demtroder, W. *Laser Spectroscopy: Basic Concepts and Instrumentation*; Springer Verlag: Berlin-Heidelberg, 2002.

(2) Huber, K. P., Herzberg, G. Constants of Diatomic Molecules. In *Molecular Spectra and Molecular Structure*; Van Nostrand Reinhold: New York, 1979; Vol. *4*.

(3) Turner, D. W. *Molecular Photoelectron Spectroscopy*; Wiley: New York, 1970.

(4) Gel'mukhanov, F.; Ågren, H.; Sałek, P. Doppler Effects in Resonant X-ray Raman Scattering. *Phys. Rev. A* **1998**, *57*, 2511−2566.

(5) Björneholm, O.; Bässler, M.; Ausmees, A.; Hjelte, I.; Feifel, R.; Wang, H.; Miron, C.; Piancastelli, M. N.; Svensson, S.; Sorensen, S. L.; et al. Doppler Splitting of In-Flight Auger Decay of Dissociating Oxygen Molecules: The Localization of Delocalized Core Holes. *Phys. Rev. Lett.* **2000**, *84*, 2826−2829.

(6) Kitajima, M.; Ueda, K.; De Fanis, A.; Furuta, T.; Shindo, H.; Tanaka, H.; Okada, K.; Feifel, R.; Sorensen, S. L.; Gel'mukhanov, F.; et al. Doppler Effect in Resonant Photoemission from SF_6: Correlation Between Doppler Profile and Auger Emission Anisotropy. *Phys. Rev. Lett.* **2003**, *91*, 213003.

(7) Travnikova, O.; Liu, J.-C.; Lindblad, A.; Nicolas, C.; Söderström, J.; Kimberg, V.; Gel'mukhanov, F.; Miron, C. Circularly Polarized X Rays: Another Probe of Ultrafast Molecular Decay Dynamics. *Phys. Rev. Lett.* **2010**, *105*, 233001.

(8) Gel'mukhanov, F.; Ågren, H. Resonant X-Ray Raman Scattering. *Phys. Rep.* **1999**, *312*, 87−330.

(9) Ueda, K. Core Excitation and De-Excitation Spectroscopies of Free Atoms and Molecules. *J. Phys. Soc. Jpn.* **2006**, *75*, 032001.

(10) Piancastelli, M. N. Auger Resonant Raman Studies of Atoms and Molecules. *J. Electron Spectrosc. Relat. Phenom.* **2000**, *107*, 1−26.

(11) Miron, C.; Morin, P. High-Resolution Inner-Shell Photoionization Photoelectron and Coincidence Spectroscopy. In *Handbook of High-Resolution Spectroscopy*; John Wiley & Sons, Ltd.: Chichester, U.K, 2011.

(12) Morin, P.; Miron, C. Ultrafast Dissociation: An Unexpected Tool for Probing Molecular Dynamics. *J. Electron Spectrosc. Relat. Phenom.* **2012**, *185*, 259−266.

(13) Gavrilyuk, S.; Sun, Y.-P.; Levin, S.; Ågren, H.; Gel'mukhanov, F. Recoil Splitting of X-ray Induced Optical Fluorescence. *Phys. Rev. A* **2010**, *81*, 035401.

(14) Simon, M.; Püttner, R.; Marchenko, T.; Guillemin, R.; Kushawaha, R. K.; Journel, L.; Goldsztejn, G.; Piancastelli, M. N.; Ablett, J. M.; Rueff, J.-P.; et al. Atomic Auger Doppler Effects upon Emission of Fast Photoelectrons. *Nat. Commun.* **2014**, *5*, 4069.

(15) Sun, Y.-P.; Wang, C.-K.; Gel'mukhanov, F. Rotational Doppler Effect in X-ray Photoionization. *Phys. Rev. A* **2010**, *82*, 052506.

(16) Thomas, T. D.; Kukk, E.; Ueda, K.; Ouchi, T.; Sakai, K.; Carroll, T. X.; Nicolas, C.; Travnikova, O.; Miron, C. Experimental Observation of Rotational Doppler Broadening in a Molecular System. *Phys. Rev. Lett.* **2011**, *106*, 193009.

(17) Miron, C.; Miao, Q.; Nicolas, C.; Bozek, J. D.; Andrałojć, W.; Patanen, M.; Simões, G.; Travnikova, O.; Ågren, H.; Gel'mukhanov, F. Site-Selective Photoemission from Delocalized Valence Shells Induced by Molecular Rotation. *Nat. Commun.* **2014**, *5*, 3816.

(18) Lavery, M. P. J.; Speirits, F. C.; Barnett, S. M.; Padgett, M. J. Detection of a Spinning Object Using Lightas Orbital Angular Momentum. *Science* **2013**, *341*, 537−540.

(19) Korech, O.; Steinitz, U.; Gordon, R. J.; Averbukh, I. S.; Prior, Y. Observing Molecular Spinning via the Rotational Doppler Effect. *Nat. Photonics* **2013**, *7*, 711−714.

(20) Lofthus, A.; Krupenie, P. H. The Spectrum of Molecular Nitrogen. *J. Phys. Chem. Ref. Data* **1977**, *6*, 113−307.

(21) Öhrwall, G.; Baltzer, P.; Bozek, J. Photoelectron Spectra of N_2^+: Rotational Line Profiles Studied with He I Excited Angle-resolved Spectroscopy and with Synchrotron Radiation. *Phys. Rev. A* **1999**, *59*, 1903−1912.

(22) Felicissimo, V. C.; Guimaraes, F. F.; Gel'mukhanov, F. Enhancement of the Recoil Effect in X-ray Photoelectron Spectra of Molecules Driven by a Strong IR Field. *Phys. Rev. A* **2005**, *72*, 023414.

DOI: 10.1021/acs.jpclett.5b00325
J. Phys. Chem. Lett. 2015, 6, 1568−1572

(23) Takata, Y.; Kayanuma, Y.; Yabashi, M.; Tamasaku, K.; Nishino, Y.; Miwa, D.; Harada, Y.; Horiba, K.; Shin, S.; Tanaka, S.; et al. Recoil Effects of Photoelectrons in a Solid. *Phys. Rev. B* **2007**, *75*, 233404.
(24) Semenov, S. K.; Cherepkov, N. A.; Matsumoto, M.; Hatamoto, T.; Liu, X.-J.; Prümper, G.; Tanaka, T.; v, M.; Tanaka, H.; Gelamukhanov, F.; et al. Interference Modulation in the Vibrationally Resolved Photoionization of the $1\sigma_g$ and $1\sigma_u$ Core Levels of the N_2. Molecule. *J. Phys. B: At. Mol. Opt. Phys.* **2006**, *39*, L261−L267.
(25) Ueda, K.; Liu, X.-J.; Prümper, G.; Lischke, T.; Tanaka, T.; Hoshino, M.; Tanaka, H.; Minkov, I.; Kimberg, V.; Gel'mukhanov, F. Role of the Recoil Effect in Two-center Interference in X-ray Photoionization. *Chem. Phys.* **2006**, *329*, 329−337.
(26) Domcke, W.; Cederbaum, L. S. Electronic Recoil Effects in High-Energy Photoelectron Spectroscopy. *J. Electron Spectrosc. Relat. Phenom.* **1978**, *13*, 161−173.
(27) Thomas, T. D.; Kukk, E.; Fukuzawa, H.; Ueda, K.; Püttner, R.; Tamenori, Y.; Asahina, T.; Kuze, N.; Kato, H.; Hoshino, M.; et al. Photoelectron-Recoil-induced Rotational Excitation of the $B^2\Sigma_u$. State in N_2. *Phys. Rev. A* **2009**, *79*, 022506.
(28) Thomas, T. D.; Kukk, E.; Ouchi, T.; Yamada, A.; Fukuzawa, H.; Ueda, K.; Puttner, R.; Higuchi, I.; Tamenori, Y.; Asahina, T.; et al. Valence Photoelectron Spectroscopy of N_2 and CO: Recoil-induced Rotational Excitation, Relative Intensities, and Atomic Orbital Composition of Molecular Orbitals. *J. Chem. Phys.* **2010**, *133*, 174312.
(29) Thomas, T. D. Small Molecule Photoelectron Spectroscopy: Recoil Effects, Stoichiometric Surprises, and Double-Core-Hole Ionization. *J. Electron Spectrosc. Relat. Phenom.* **2013**, *189*, 3−10.
(30) Gel'mukhanov, F.; Carravetta, V.; Ågren, H. Channel Interference in Resonant Auger Scattering by Surface Adsorbed Molecules. *Phys. Rev. B* **1998**, *58*, 2216−2227.
(31) Cohen, H. D.; Fano, U. Interference in the Photo-Ionization of Molecules. *Phys. Rev.* **1966**, *150*, 30−33.
(32) Miron, C.; Kimberg, V.; Morin, P.; Nicolas, C.; Kosugi, N.; Gavrilyuk, S.; Gel'mukhanov, F. Vibrational Scattering Anisotropy Generated by Multichannel Quantum Interference. *Phys. Rev. Lett.* **2010**, *105*, 093002.
(33) Canton, S. E.; Plesiat, E.; Bozek, J. D.; Rude, B. S.; Decleva, P.; Martin, F. Direct Observation of Young's Double-Slit Interferences in Vibrationally Resolved Photoionization of Diatomic Molecules. *Proc. Natl. Acad. Sci. U.S.A.* **2011**, *108*, 7302−7306.
(34) Argenti, L.; Thomas, T. D.; Plesiat, E.; Liu, X. J.; Miron, C.; Lischke, T.; Prumper, G.; Sakai, K.; Ouchi, T.; Puttner, R.; et al. Double-Slit Experiment with a Polyatomic Molecule: Vibrationally-Resolved C 1s Photoelectron Spectra of Acetylene. *New. J. Phys.* **2012**, *14*, 033012.
(35) Kushawaha, R. K.; Patanen, M.; Guillemin, R.; Journel, L.; Miron, C.; Simon, M.; Piancastelli, M. N.; Skates, C.; Decleva, P. From Double-slit Interference to Structural Information in Simple Hydrocarbons. *Proc. Natl. Acad. Sci. U.S.A.* **2013**, *110*, 15201−15206.
(36) Liu, X. J.; Miao, Q.; Gel'mukhanov, F.; Patanen, M.; Travnikova, O.; Nicolas, C.; Ågren, H.; Ueda, K.; Miron, C. Einstein-Bohr Recoiling Double-Slit Gedanken Experiment Performed at the Molecular Level. *Nat. Photonics* **2015**, *9*, 120−125.
(37) Miron, C.; et al. PLÉIADES Beamline. http://www.synchrotron-soleil.fr/Recherche/LignesLumiere/PLEIADES.
(38) Kimberg, V.; Lindblad, A.; Söderström, J.; Travnikova, O.; Nicolas, C.; Sun, Y. P.; Gel'mukhanov, F.; Kosugi, N.; Miron, C. Single-Molecule X-ray Interferometry: Controlling Coupled Electron-Nuclear Quantum Dynamics and Imaging Molecular Potentials by Ultrahigh Resolution Resonant Photoemission and ab initio Calculations. *Phys. Rev. X* **2013**, *3*, 011017.
(39) Wuerker, R. F.; Schmitz, L.; Fukuchi, T.; Straus, P. Lifetime Measurements of the Excited States of N_2 And N_2^+ by Laser-induced Fluorescence. *Chem. Phys. Lett.* **1998**, *150*, 443−446.
(40) Verner, D. A.; Yakovlev, D. G. Analytic Fits for Partial Photoionization Cross Sections. *Astron. Astrophys., Suppl. Ser.* **1995**, *109*, 125−157.
(41) Frisch, M. J., Trucks, G. W., Schlegel, H. B., Scuseria, G. E., Robb, M. A., Cheeseman, J. R., Scalmani, G., Barone, V., Mennucci, B., Petersson, G. A. et al. *Gaussian 09*, revision A.02; Gaussian, Inc.: Wallingford, CT, 2009.

DOI: 10.1021/acs.jpclett.5b00325
J. Phys. Chem. Lett. 2015, 6, 1568−1572